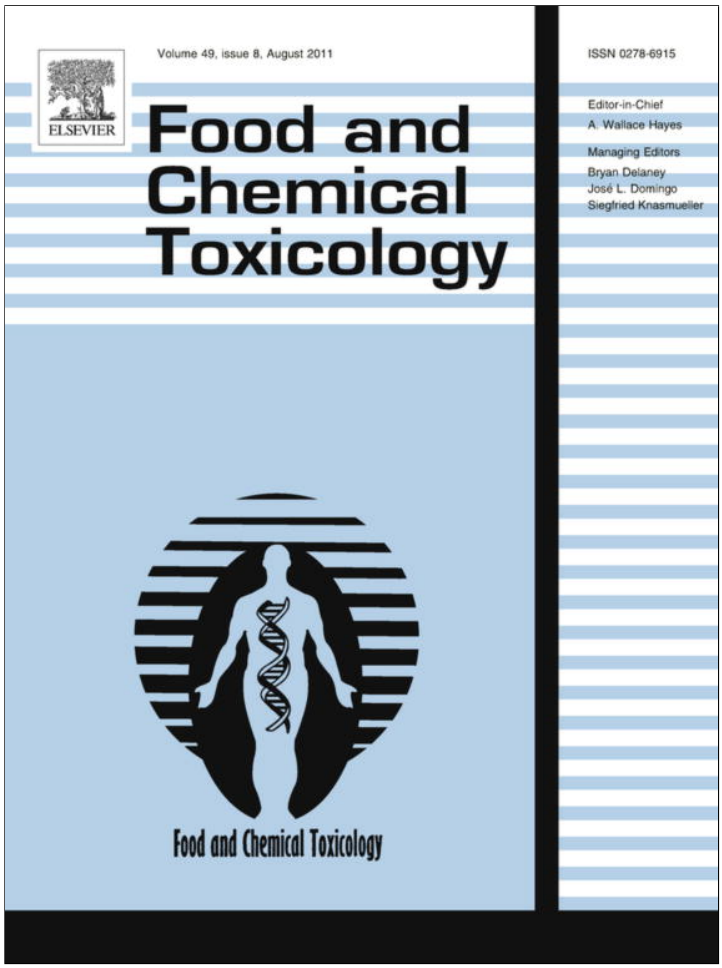

Food and Chemical Toxicology 49 (2011) 1787–1795

Contents lists available at ScienceDirect

Food and Chemical Toxicology

journal homepage: www.elsevier.com/locate/foodchemtox

Preferential binding of insecticide phorate with sub-domain IIA of human serum albumin induces protein damage and its toxicological significance

Quaiser Saquib [a,b], Abdulaziz A. Al-Khedhairy [a,b], Maqsood A. Siddiqui [a], Atanu Singha Roy [d], Swagata Dasgupta [d], Javed Musarrat [a,b,c,*]

[a] A.R. Al-Jeraisy Chair for DNA Research, College of Science, King Saud University, Riyadh 11451, Saudi Arabia
[b] Department of Zoology, King Saud University, P.O. Box 2455, Riyadh 11451, Saudi Arabia
[c] Department of Microbiology, Faculty of Agricultural Sciences, AMU, Aligarh, India
[d] Department of Chemistry, Indian Institute of Technology, Kharagpur 721302, India

ARTICLE INFO

Article history:
Received 5 February 2011
Accepted 15 April 2011
Available online 1 May 2011

Keywords:
Human serum albumin
Phorate
Insecticide
Fluorescence spectroscopy
Molecular modeling
Cytotoxicity

ABSTRACT

Phorate, an organophosphorus insecticide is known for its adverse effects on acetylcholinesterase, and other neuronal and pulmonary activities. Most likely, the toxicity of drugs/agrochemicals is modulated through cellular distribution bound to plasma proteins. Therefore, the *in vitro* interaction of phorate with human serum albumin (HSA) has been investigated, using sensitive techniques like fluorescence spectroscopy and circular dichroism, to ascertain its binding mechanism and toxicological implications. Fluorescence studies revealed the quenching constant (Ksv) as $2.5 \times 10^4\ M^{-1}$ and binding affinity (Ka) as $2.96 \times 10^4\ M^{-1}$ ($r^2 = 0.99$), with a primary binding site of phorate at sub-domain IIA of HSA. Circular dichroism (CD) data demonstrated a noticeable reduction in secondary structure (α-helical content) of phorate treated HSA. Albumin treated with 200–1000 μM phorate released significant amounts of acid soluble amino and carbonyl groups, whereas higher concentrations resulted in protein fragmentation. It is postulated that the 1′-O and 3-O alkyl groups of phorate have a role in binding with electrophilic centers of Trp 214, and Arg 218/Lys 195, respectively. Moreover, the significant ultrastructural changes, reactive oxygen species (ROS) generation, mitochondrial damage and cell death in phorate treated cultured human amnion epithelial (WISH) cells, elucidated phorate induced cellular toxicity.

1. Introduction

The organophosphorus compound O,O-diethyl s-ethylthiomethyl phosphorodithioate (CAS No. 298-02-2) commonly known as phorate, is a systemic insecticide generally applied for protection against aphides and viral diseases in different field crops (Abhilash and Singh, 2009). It is categorized as a Class I, high-risk toxic compound by Environmental Protection Agency (EPA), and Pest Management Regulatory Agency Health (PMRAH) (http://extoxnet.orst.edu/pips/phorate.htm; PMRAH, 2003). Phorate is known to inhibit the activity of acetylcholinesterase enzyme by phosphorylation of the serine hydroxyl group in the substrate binding domain of the enzyme resulting in accumulation of acetylcholine and associated neurotoxicity (Vandana and Zzaman, 1997; Fulton and Key, 2001; Oruc and Usta, 2007). It also adversely affect the activity of CYP1A2 and CYP3A4 cytochrome P450 (CYP) monooxidases, and consequently manifest the toxicity symptoms in non-target organisms (Kashyap et al., 1984), including the increased risk of prostate cancer (Alavanja et al., 2003; Mahajan et al., 2006). In biological system, it is transformed into highly toxic metabolites of oxon by the enzyme CYP450 (Henderson et al., 2004; Usmani et al., 2004), and may cause pulmonary toxicity in exposed individuals (Henderson et al., 2004; Kashyap et al., 1984). However, in spite of the associated human health hazards, phorate is still being used in agriculture practices in many countries (Zambonin et al., 2004; Pagliuca et al., 2006; Wang et al., 2008), and its residues have been detected in various food commodities (Mansour et al., 2009a,b; Wang et al., 2008; Pagliuca et al., 2006). Lately, Mansour et al. (2009a) have reported phorate as a potential risk to human health due to consumption of contaminated potatoes and other vegetables containing 2.2 and 2.68-fold higher levels of phorate residues, as compared to the WHO acceptable daily intake (ADI) limit of 0.0005 mg kg bw/d.

Toxicity of phorate has been studied both in the *in vitro* test systems, as well as in animal and humans (Sobti et al., 1982; Mahli and Grover, 1987; DeFerrari et al., 1991; Morowati, 2001). Furthermore, the reports on interactions of several pesticides, as exogenous ligands, with biological macromolecules, and their extent and nature of binding are also available in literature (Jaiswal et al., 2002; Silva et al., 2004; Zhang et al., 2007; Saquib et al.,

* Corresponding author at: A.R. Al-Jeraisy Chair for DNA Research, Department of Zoology, College of Science, P.O. Box 2455, King Saud University, Riyadh 11451, Saudi Arabia. Tel.: +966 4675768; fax: +966 4675514.
E-mail address: musarratj1@yahoo.com (J. Musarrat).

0278-6915/$ - see front matter © 2011 Elsevier Ltd. All rights reserved.
doi:10.1016/j.fct.2011.04.028

2010a). Our earlier studies on a herbicide paraquat–BSA interactions demonstrated the binding constant (Ka) and binding capacity (n) of albumin as $3.4 \times 10^5\ M^{-1}$ and 12.9, respectively (Jaiswal et al., 2002). Also, a recent report on the interaction of a fungicide methyl thiophanate (MT) with human serum albumin (HSA) suggested the binding affinity (Ka) and capacity (n) of HSA as $1.65 \times 10^4\ M^{-1}$ and 1.0 ($r^2 = 0.99$), respectively (Saquib et al., 2010a). Nevertheless, to the best of our understanding, the information on interaction of phorate and its effects on structural integrity of biological macromolecules (protein and/or DNA) and cells per se are not adequately cited in literature.

Therefore, this study for the first time elucidated the mechanistic aspects of phorate induced structural damage in HSA and its toxicological significance. The results provided vital information on the (i) extent and nature of interactions of phorate with HSA (ii) binding constant (Ka) and number of phorate binding sites (n) on HSA, (iii) phorate induced conformational changes leading to protein damage, and (iv) ROS generation and mitochondrial damage as oxidative stress markers, to explicate the plausible mechanism of phorate–HSA interaction and its toxicological implications.

2. Material and methods

2.1. Materials

Human serum albumin (HSA) fraction V-fatty acid free, acrylamide, *N,N′*-methylenebisacrylamide, TEMED, low range (6500–66,000 Da) lyophilized protein marker, glycine, bilirubin, dimethyl sulfoxide (DMSO), Coomassie brilliant blue R-250, Tris (hydroxymethyl) aminomethane were purchased from Sigma Chemical Company (USA). All other chemicals were obtained from E. Merck, Darmstadt (Germany). Phorate, (95% pure) (Fig. 1) was a kind gift from Agrochemical Division, Indian Agriculture Research Institute (India). The stock solution of phorate was prepared in DMSO. All experiments were performed using MilliQ water and all the stock solutions were filtered through 0.45 μm Millipore filters prior to mixing, to minimize the inner filter effect (Chignell, 1972).

2.2. Phorate–HSA fluorescence measurements

Fluorescence measurements were carried out on a Shimadzu spectrofluorophotometer, model RF5301PC equipped with RF 530XPC instrument control software, at ambient temperature. The fluorescence spectra of HSA (3 μM) alone were recorded by fixing the excitation and emission slits at 3 nm each with a 1 cm path length cell. The emission spectra of HSA were recorded in the range of 290–380 nm and the excitation wavelength was set at 280 nm. However, phorate does not fluoresce at the above excitation and emission wavelengths. Fluorescence studies were done by titrating HSA with increasing concentrations of phorate. In brief, to a fixed concentration (3.0 μM) of protein solution, varying amounts of phorate were added to obtain the molar ratios in the range of 1:1 to 1:11. Fluorescence quenching of HSA was determined using the Stern–Volmer equation (Eq. (1)) as described by Saquib et al. (2010a).

$$F_0/F = 1 + \mathrm{Ksv}[Q] \quad (1)$$

Where F_0 and F denote the fluorescence intensities in the absence and presence of quencher (phorate), respectively, Ksv is the Stern–Volmer quenching constant, and [Q] is the concentration of quencher. Therefore, Eq. (1) was applied to determine Ksv by linear regression of a plot of F_0/F vs [Q]. Furthermore, the binding constant (Ka) and number of bound phorate to HSA (n) were determined by plotting the double log graph of the fluorescence data using equation (Eq. (2)),

$$\log(F_0 - F)/F \text{ vs } \log Ka + n \log[Q] \quad (2)$$

Also, the binding constant was calculated from the modified Stern–Volmer equation (Eq. (3))

$$F_0/\Delta F = 1/\mathrm{fa}\,\mathrm{Ka}[Q] + 1/\mathrm{fa} \quad (3)$$

where F_0 and F are the relative fluorescence intensities in absence and presence of the quencher, respectively, $\Delta F = F_0 - F$; fa is the fraction of the initial fluorophore accessible to the quencher, [Q] the quencher concentration, and Ka is the quenching constant.

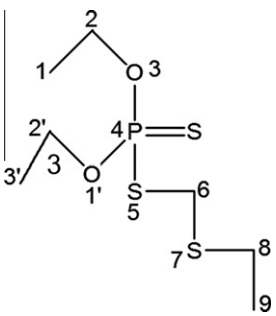

Fig. 1. Structure of phorate.

2.3. Synchronous fluorescence analysis of phorate treated HSA

In order to determine the induced structural changes in HSA with the addition of phorate, synchronous fluorescence analysis has been performed. In brief, a fixed concentration of HSA (3 μM) was titrated with phorate at varying molar ratios (1:1 to 1:10). The wavelength ranges selected for synchronous scanning were 310–370 nm ($\Delta\lambda$ = 60 nm) and 280–330 nm ($\Delta\lambda$ = 15 nm).

2.4. Site specific binding of phorate on HSA using marker ligand

The specific binding of phorate on HSA molecule was studied with bilirubin, which specifically binds to site I on HSA molecule. Changes in fluorescence intensity of HSA–phorate complex were monitored at 340 nm after excitation at 280 nm with the addition of varying amounts of marker ligand. The percent reduction in fluorescence intensity upon marker ligand binding was calculated considering the fluorescence intensity of phorate–HSA complex as 100%.

2.5. Circular dichroism (CD) measurements

Effect of phorate on the native conformation of HSA was analyzed by treating HSA at a fixed concentration of 4.5 μM with 0.1 and 0.2 μM of phorate to get the phorate–HSA molar ratio of 1:0.02 and 1:0.04. The untreated and phorate treated samples were incubated for 2 h in white light at 37 °C. CD measurements were carried out on a Jasco spectropolarimeter, model J-815, Japan. The CD measurements were carried out accordingly, as described by Saquib et al. (2010a). The results were expressed as mean residue ellipticity (MRE) in deg cm^2 $dmol^{-1}$, which is defined as [MRE = θ obs (mdeg)/$10 \times n \times l \times$ Cp]. The θ obs represents the ellipticity in millidegree, n is the number of amino acid residues (585), l is the path length of the cell in cm and Cp is the mole fraction. The α-helical content of HSA was calculated from the MRE value at 222 nm using the equation %helix = [(MRE222 − 2340)/30,300] × 100, as described by Chen et al. (1972).

2.6. Phorate induced fragmentation of serum albumin

Damage to HSA was assessed by measuring the TCA soluble amino groups and carbonyl groups released from treated serum albumin according to the method of Moore and Stein (1954), and Lappin and Clark (1951). SDS–polyacrylamide gel electrophoresis of untreated and phorate treated HSA was carried out on 10% (w/v) gel, according to the method of Laemmli (1970). In brief, HSA (25 μg) was treated with increasing concentrations (1–5 mM) of phorate for 2 h at 37 °C. The aliquots (6 μg each) of untreated control and treated protein were loaded on the gel and run at 3 mA per well for 3 h. Gel stained with Coomassie brilliant blue was visualized on UVP GelDoc-It imaging system (UVP Ltd.,UK).

2.7. Molecular modeling of phorate–HSA interaction

The crystal structure of HSA (PDB ID 1AO6) was downloaded from the Protein Data Bank (PDB) (Berman et al., 2000). The energy minimized structure of phorate was generated using Sybyl 6.92 (Tripos Inc., St. Louis, USA) using the Tripos force field and MMFF94 charges with a gradient of 0.005 kcal mol^{-1}. The number of iterations and the dielectric constant were set to 1000 and 1.0 respectively. The FlexX programme that is part of the Sybyl suite was used to perform the docking of phorate with HSA. The docked conformation of phorate in HSA was visualized using PyMol (Delano, 2004). The accessible surface area (ASA) free and complexed HSA was calculated with NACCESS (Hubbard and Thornton, 1993). The change in ASA for the residue n was calculated using $\Delta ASA^n = ASA^n$ (free HSA)–ASA^n (phorate–HSA). It was assumed that if the loss in ASA of a residue is greater than 10 $Å^2$, then it is most likely involved in the interaction.

2.8. Determination of extracellular ROS generation by NBT assay

Superoxide anions were estimated by nitrobluetetrazolium (NBT) reduction assay according to the method of Nakayama et al. (1983). In brief, the reaction mixture containing 100 mM Tris–HCl buffer (pH 7.2), 50 μM NBT, 100 μM EDTA,

0.06% Triton X-100 was mixed with varying concentrations (100–1000 μM) of phorate. The tubes containing reaction mixture were exposed to white light (20 W/m^2) for 2 h. Parallel reaction with phorate was run in dark. The absorbance of blue color developed was read at 560 nm using Cintra 10e UV–vis spectrophotometer and plotted as a function of phorate concentration.

2.9. Determination of intracellular ROS generation in WISH cells

Assessment of phorate induced intracellular ROS generation was performed on human amnion epithelial (WISH) cell line using fluorescent probe DCFH-DA (Saquib et al., 2010b). In brief, the WISH cells were grown in RPMI 1640 supplemented with 10% FBS and antibiotic–antimycotic solution (100×, 1 ml/100 ml of medium) in 5% CO_2 with 95% atmosphere in humidity at 37 °C, accordingly as described by Siddiqui et al. (2010). Each batch of cells was assessed for cell viability by trypan blue dye exclusion test prior to experiment and batches showing more than 95% cell viability were used in the study. The cells were treated with increasing concentrations of phorate (50–1000 μM) for 72 h at 37 °C in 5% CO_2 atmosphere. Untreated cells were also run in parallel. The cells were then visualized under fluorescence microscope (Nikon, Eclipse E600) at the excitation and emission wavelengths of 485 and 530 nm, respectively.

2.10. Detection of mitochondrial damage in WISH cells

Mitochondrial damage was monitored by observing the changes in the fluorescence intensity of mitochondria specific dye rhodamine (Rh123) in WISH cells, as described by Saquib et al. (2010b). The untreated control cells and those treated with phorate in concentration range of (50, 100, 250, 500 and 1000 μM) for 72 h at 37 °C were stained with 20 μM Rh123 for 1 h at 37 °C, and visualized under fluorescence microscope (Nikon, Eclipse E600) at the excitation wavelength of 520 nm and emission wavelength of 590 nm.

2.11. TEM analysis of phorate treated human cells

Ultrastructural changes in the phorate treated cultured human epithelial amnion (WISH) cells were studied with transmission electron microscopy (TEM) using the method of Saquib et al. (2010b). In brief WISH cells were exposed to 500 and 1000 μM phorate for 72 h at 37 °C. Subsequently, the ultrathin sections of glutaraldehyde fixed untreated and phorate treated cells, embedded in low viscosity araldite resin were prepared, and visualized under high vacuum at 100 kV using JEOI-1011 electron microscope (JEOL, Japan).

3. Results

3.1. Fluorescence quenching of HSA upon phorate interaction

Effect of phorate on HSA molecule was measured by monitoring the changes in the intrinsic fluorescence of serum albumin at different phorate–HSA molar ratios. The fluorescence emission spectra of HSA alone and in presence of varying molar ratios (11:1) of phorate–HSA were recorded in the range of 290–380 nm. Fig. 2A shows the fluorescence decay curves of the free HSA and phorate–HSA complex. The titration curves exhibited a pronounced shift of 29 nm towards shorter wavelength in the emission maxima (λ_{em}) of HSA. The fluorescence intensity of phorate in the range of 290–380 nm was found to be non-significant as compared with HSA fluorescence. Fig. 2B shows the Stern–Volmer plot of the quenching of HSA fluorescence by phorate. The quenching constant (Ksv) were determined to be 2.5 × 10^4 M^{-1} (r^2 = 0.99). Based on the double log plot of the fluorescence data, the binding constant (Ka) and number of binding sites (n) on HSA were determined to be 2.96 × 10^4 M^{-1} and 1.02 (r^2 = 0.99), respectively (Fig. 3A). Furthermore, the binding characteristics were revalidated with the modified Stern–Volmer plot of F_0/F vs 1/[Q] (Fig. 3B) and a reproducible binding constant (2.94 × 10^4 M^{-1}) has been obtained.

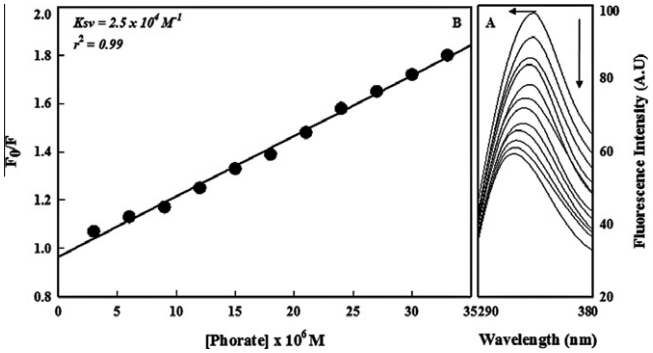

Fig. 2. Fluorescence quench titration of phorate with HSA. Panel A depicts fluorescence emission spectra of HSA in the absence (uppermost curve) and presence of increasing amounts of phorate. The spectra were obtained in 10 mM Tris–HCl buffer, pH 7.4 at ambient temperature. Varying concentrations of phorate to HSA were: (top to bottom) 0.0, 3, 6, 9, 12, 15, 18, 21, 24, 27, 30 and 33 respectively. Fluorescence decay is indicated by down arrow (↓) and shift in the emission spectra is shown by horizontal (←) arrow. Panel B represents the Stern–Volmer plot showing the fluorescence quenching of HSA as a function of phorate concentration.

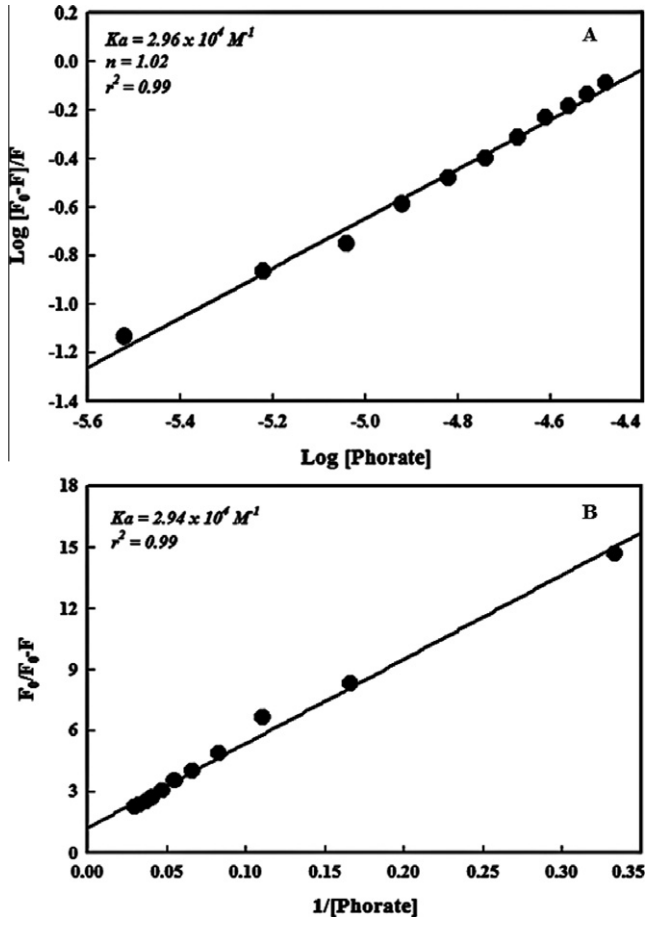

Fig. 3. Binding isotherms representing the affinity and extent of phorate–HSA interaction. Panels A and B show the double-logarithmic plot and modified Stern–Volmer plot, respectively for determining the binding constant (Ka) and number of binding sites (n) of phorate on HSA molecule.

3.2. Site-specific binding of phorate on HSA molecule

The competitive displacement of phorate from phorate–HSA complex with the addition of bilirubin at the increasing molar ratios of 1:0.25, 1:0.5 and 1:1, demonstrated the site-I specific binding of phorate on HSA molecule. The emission spectra of phorate–HSA complex at 340 nm showed significant reduction in HSA fluorescence upon addition of bilirubin, with a shift of 10 nm in the emission maxima (Fig. 4A). The total percentage decline in fluorescence quenching of phorate–HSA complex with the addition of bilirubin has been determined to be 33.83% at 1:1 molar ratio (Fig. 4B). However, the addition of diazepam at the same molar

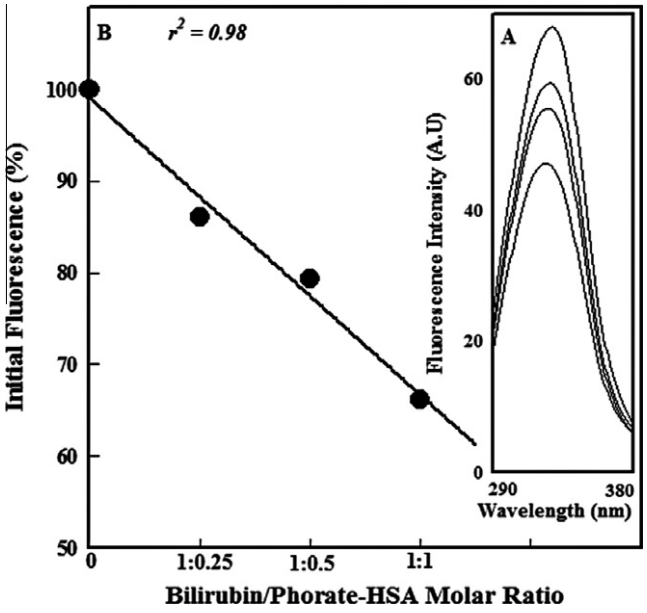

Fig. 4. Competitive binding of phorate with HSA in presence of bilirubin as a site-I marker ligand. Panel A represents the fluorescence quenching of phorate–HSA complex with increasing concentrations of bilirubin. Spectra from top to bottom: phorate–HSA complex (10:1), bilirubin–HSA molar ratios of 0.25, 0.5 and 1.0. Panel B shows decline in the initial fluorescence of phorate–HSA (10:1) complex with the addition of increasing molar ratios of bilirubin as a site I marker.

ratios has not exhibited any reduction in the emission spectra of phorate–HSA complex (results not shown).

3.3. Conformational analysis of HSA upon interaction with phorate

The conformational changes of HSA were evaluated by recording the synchronous fluorescence intensity of protein before and after addition of phorate. Synchronous fluorescence spectra provided the information about changes in the molecular microenvironment in vicinity of the fluorophore functional groups. With the stabilization of $\Delta\lambda$ values (scanning interval, $\Delta\lambda = \lambda$ emission $- \lambda$ excitation) at 15 or 60 nm, the synchronous fluorescence of HSA, yields the specific information on ligand binding with tyrosine and tryptophan residues, respectively. In the synchronous fluorescence of HSA, shift in position of maximum emission wavelength corresponds to the changes of polarity around the fluorophore of amino acid residues. The effect of phorate on HSA synchronous fluorescence is shown in Fig. 5A and B. At the highest HSA–phorate molar ratio of 1:10, the tryptophan fluorescence was declined to 1.4-fold, as compared to 1.17-fold reduction in the fluorescence intensity of tyrosine residue. The results in Fig. 5A show that the fluorescence of tyrosine residues is weak and the position of maximum emission wavelength had no change, when $\Delta\lambda$ was 15 nm. However, the fluorescence of tryptophan residues was higher and the maximum emission wavelength shows a moderate red shift when $\Delta\lambda$ was 60 nm (Fig. 5B).

3.4. Assessment of structural alterations in HSA upon phorate treatment by CD analysis

Titration of HSA with phorate has been optimized to achieve the molar ratios of 1:0.02 and 1:0.04 for recording the characteristic HSA spectra. Since phorate also absorbs in the spectral range of 200–250 nm at concentrations above 0.1 μM, the lower molar ratios were opted for CD analysis as compared to fluorescence studies, in order to overcome the phorate spectral interference without compromising the impact of phorate on HSA secondary structure. CD being a sensitive technique picked up the signals even at the lower molar ratios and the spectra of HSA exhibited two negative bands in the ultraviolet region at 209 and 222 nm, characteristic for α-helical structure of protein (Fig. 6A). A concentration dependent change in the ellipticity value has been recorded. The significant reductions in the MRE reflect the alterations in protein helicity. The percent changes in the α-helical content of the protein are shown in Fig. 6B. At a molar ratio of 1:0.04, the perturbation has been determined to be 6.55% with loss in protein helicity from 54.8% in native untreated HSA to 51.2% upon phorate treatment.

3.5. Phorate induced fragmentation of HSA

The quantitative spectrophotometric assays of carbonyl and acid soluble amino groups released from phorate treated HSA indicated the phorate induced HSA damage. Treatment of HSA at the varying concentrations of 200, 400, 600, 800 and 1000 μM of phorate for 2 h resulted in the release of 48.0, 82.4, 104.9, 179.4 and 215.7 μM carbonyl groups, respectively (Fig. 7A). Also, the increase in absorbance of blue color developed due to acid soluble amino groups was noticed up to 1000 μM phorate at 570 nm. The absolute amount of acid soluble amino groups released from the phorate treated HSA at 200, 400, 600, 800 and 1000 μM were determined to be 0.49, 1.29, 1.82, 2.74 and 3.6 μM, respectively (Fig. 7B). Although the protein fragmentation was not apparent on SDS–PAGE at lower concentrations, however, the disappearance of parent bands was noticed at a higher dose range of 1–5 mM phorate (Fig. 8A). Furthermore, the densitometric analysis of the bands

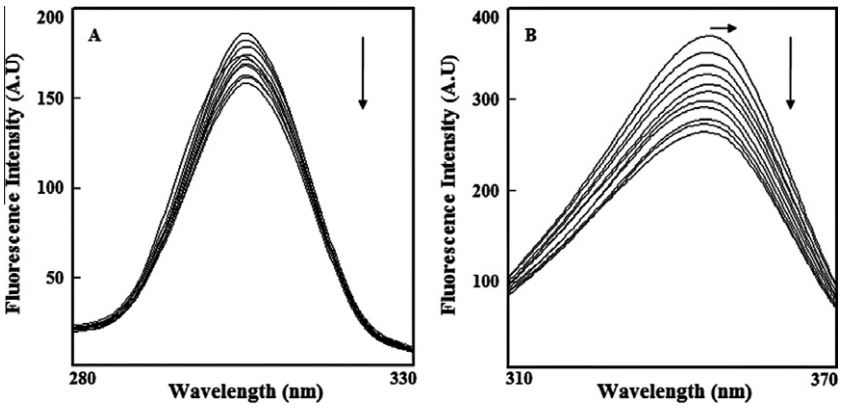

Fig. 5. Synchronous fluorescence spectra of HSA in the absence and presence of phorate. Panels A: $\Delta\lambda = 15$ and B $\Delta\lambda = 60$. From top to bottom HSA (3.0 μM), phorate: 3, 6, 9, 12, 15, 18, 21, 24, 27 and 30 μM, respectively. Fluorescence decay and shift in the emission spectra are indicated by down and horizontal arrows.

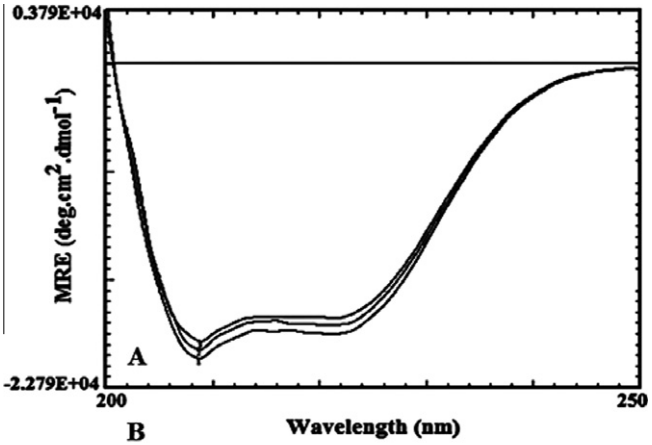

Phorate-HSA molar ratio	MRE_{222} (deg.cm^2.dmol^{-1})	α-helix	% perturbation
HSA (1:0)	18950	54.81	-
HSA-Phorate (1:0.02)	18324	52.75	3.75
HSA-Phorate (1:0.04)	17861	51.22	6.55

Fig. 6. CD spectra of HSA at different phorate concentrations bottom to top: (curve 1) Free HSA, (curve 2) phorate 0.1 μM, (curve 3) phorate 0.2 μM. The CD parameters are specified in the table underneath.

on the gel revealed a phorate concentration dependent decline in the intensity of the HSA bands with 75% loss of band intensity, at 4 mM phorate (Fig. 8B).

3.6. Docking analysis of phorate–HSA interaction

Fig. 9A shows the docked conformation of phorate with HSA. The docking pose exhibited that the phorate molecule could be accommodated in the hydrophobic cavity of sub-domain IIA in Sudlow's site I formed by helices. Apart from the interaction of phorate 1′-O with Trp 214, it is important to note that 3-O atom is also possibly involved in the hydrogen bond formation with hydrophobic residues viz. Lys 195, Lys 199, Arg 218 and Arg 222 of sub-domain IIA of HSA. The changes in ASA upon interaction of phorate with different residues of HSA are presented in Fig. 9B.

3.7. Phorate induced ROS generation and mitochondrial damage

Fig. 10A exhibits extracellular superoxide anion (O_2^-) generation upon photoexcitation of phorate in presence of NBT. The absolute amounts of O_2^- anion were estimated to be 14.0, 24.6, 50.6, 64.0, 76.0, 90.0, 102.0, 117.0, 131.0 μM at 100, 200, 300, 400, 500, 600, 800, 900 and 1000 μM phorate, respectively on exposure to white light as compared to 62.4 μM O_2^- anions generated in dark at the highest concentration of 1000 μM. The intracellular ROS have also been assessed based on detection of peroxide-dependent oxidation of DCFHDA to fluorescent 2′,7′-dichlorofluorescin (DCF) in phorate treated cultured WISH cells. Qualitative analysis revealed a concentration dependent increase in the fluorescence intensity of DCF in phorate treated cells as compared to the untreated control cells (Fig. 10B). However, at higher concentrations of 500 and1000 μM phorate, the fluorescence intensity of DCF was substantially reduced due to decrease in the number of cells because of cell death. Furthermore, the changes in mitochondrial activity, using a cationic fluorescent probe Rh123, have been noticed through fluorescence microscopic analysis of phorate treated WISH cells. The probe accumulates electrophoretically in the strong negatively charged matrix

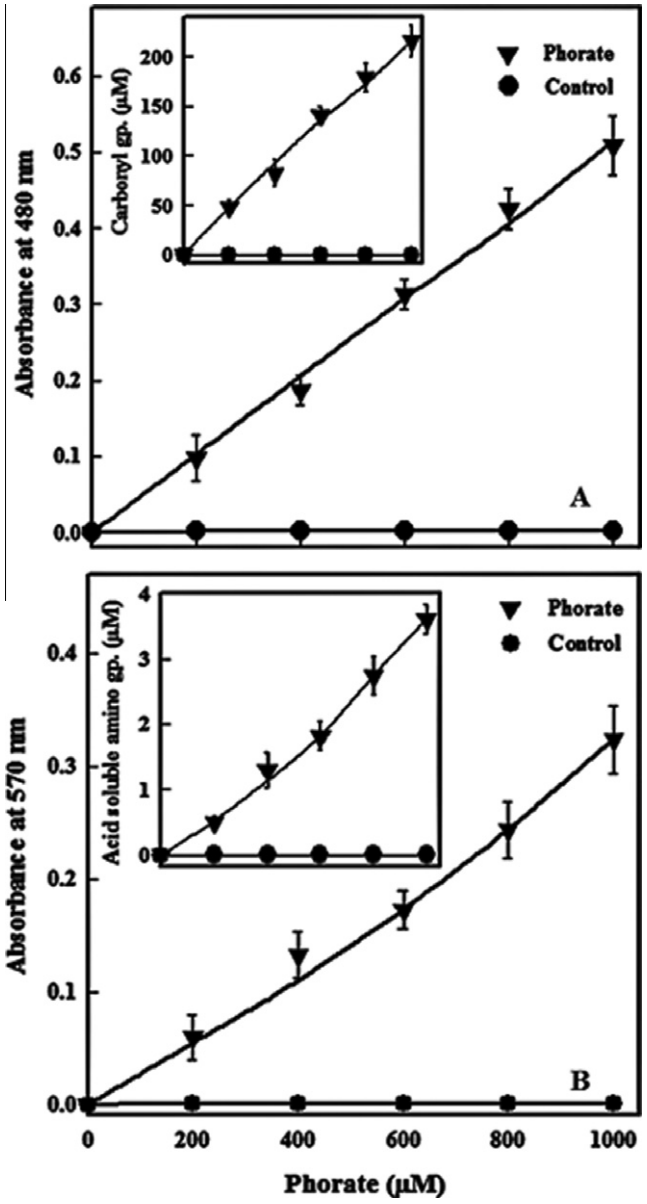

Fig. 7. Damage to HSA induced at lower phorate concentrations. Panels show the release of carbonyl groups and acid-soluble amino groups, respectively from photosensitized phorate treated HSA. The data represent the mean ± S.D. of three independent experiments done in duplicate.

of mitochondria in control cells, whereas it undergoes a phorate concentration dependent reduction in the mitochondrial fluorescent intensity, as observed in Fig. 10C. The ultrastructural TEM images of phorate treated cells are shown in Fig. 10D and supplementary Fig. 1S. The results clearly indicate the disappearance of cristae at 500 μM and cellular damage at 1000 μM phorate.

4. Discussion

Albumin being the most abundant serum protein and a major pharmaceutical drugs carrier in the blood has high accessibility to bind with a variety of electrophiles. This necessitate an in-depth investigation with the aim of determining the extent of binding of hazardous chemicals/xenobiotics, and consequent macromolecular damage relevant to the management of food and environmental chemical toxicity. Therefore, the interaction of an insecticide phorate with HSA has been probed in this study by measuring the

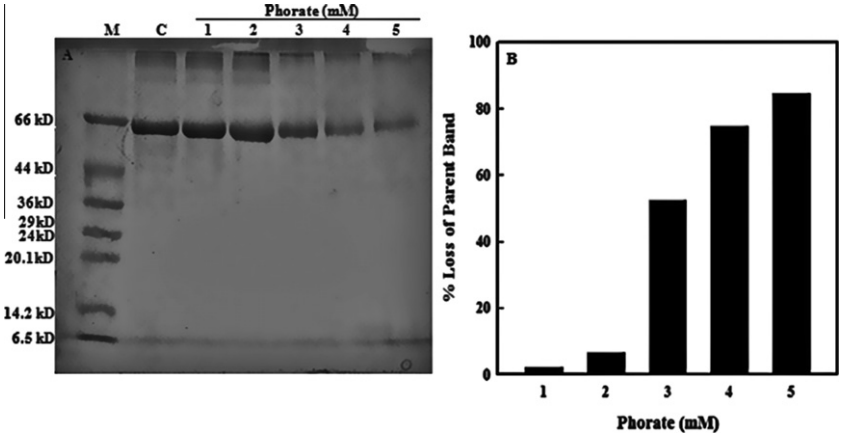

Fig. 8. HSA fragmentation at higher phorate concentrations. Panel A: SDS–polyacrylamide gel of phorate treated HSA, representing the lanes in the gel as, M: molecular size marker; C: untreated control HSA (6 μg); lanes 1–5: HSA treated with 1, 2, 3, 4 and 5 mM of phorate, respectively. Panel B: Histogram representing the densitometric analysis of the HSA bands in the lanes 1–5 indicating the loss of parental band with increasing concentrations of phorate.

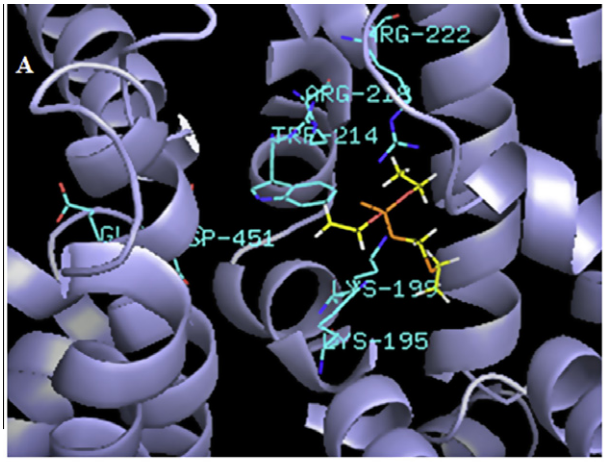

B

Residues (HSA)	Distances (Å) (Phorate)	ΔASA (Å²)	Location
Lys 195 Nε	3.68 [3-O]	45.68	IB-h4
Lys 199 Nε	4.92 [1'-O]	23.18	IB-h4
Trp 214 Nε	8.87 [1'-O]	16.5	IIA-h2
Arg 218 (Nη1)	6.15 [3-O]	15.05	IIA-h2
Arg 222 (Nη1)	2.77 [3-O]	28.99	IIA-h2

Fig. 9. Docking pose of energy-minimized structure of phorate–HSA complex. Panel A represents the stereo view of a docked pose of phorate with HSA. Panel B show the distance and accessible surface area (ΔASA) of phorate functional groups with amino acid residues of HSA.

changes in the intrinsic fluorescence of serum albumin at different phorate–HSA molar ratios. The data revealed strong quenching effect accompanied with a prominent shift in emission peaks towards the shorter wavelength, which corroborates well with the earlier reports on HSA binding with other small ligands (Li et al., 2009; Saquib et al., 2010a). This could be attributed to the changes in microenvironment of aromatic amino acids in a protein chain. The fluorescence quench titration based on the Stern–Volmer algorithm suggested that the quenching could be either dynamic or static. The changes around the single tryptophan residue located at 214 position induce conformational deformity in the sub-domain IIA (site I) of HSA molecule, causing loosening of its native structure, as also reported earlier with other pesticides (Yuan et al., 2007; Saquib et al., 2010a). Phorate induced conformational alterations in the native structure of HSA have been further substantiated by the synchronous fluorescence spectroscopy, which has exhibited relatively higher fluorescence quenching of tryptophan residue along with a moderate shift in the emission wavelength. Perturbations within the microenvironment of aromatic amino acids have been assessed by measuring the possible shift in wavelength emission maxima (λmax), which corresponds to the changes of the polarity around the chromophore molecule (Yuan et al., 1998). When the $\Delta\lambda$ values between excitation and emission wavelength were stabilized at 15 or 60 nm, the synchronous fluorescence provides the characteristic information about the 18 tyrosine and one tryptophan residues (Tang et al., 2006; Abert et al., 1993). Thus, the observed shift in the emission spectra of synchronous fluorescence signifies that phorate binds to tryptophan in the hydrophobic cavity and induces structural alterations in HSA, whereby the polarity is increased and hydrophobicity is reduced.

Furthermore, the site specific binding of phorate on sub-domain IIA of HSA molecule has been validated by competitive binding experiments. The competitive binding of phorate–HSA complex with bilirubin as a site I marker (Tayyab et al., 2003; Saquib et al., 2010a) exhibited 33.38% reduction in the fluorescence of phorate–HSA complex, which has explicitly suggested phorate binding on site I of HSA molecule. Molecular docking analysis also supported the phorate binding to hydrophobic site I (sub-domain IIA), where Trp 214 residue is located. The proposed mechanism of interaction suggests the principle role of Trp 214 in intrinsic fluorescence of HSA, and the primary involvement of 1′-O alkyl group of phorate in binding with aromatic ring of Trp 214 is envisaged as has been elucidated in Scheme 1. Moreover, the thermodynamic parameters such as the free energy (ΔG) due to ligand binding also provide an insight into the binding mode. The negative ΔG value of −5.989 kcal/mol for interaction of HSA with phorate indicates the spontaneity of the complexation. The interaction process has been found to be entropy driven and the major contribution of ΔG comes from positive ΔS. For phorate both the ΔH and ΔS (6.013 kcal/mol and 0.171 J/mol, respectively) were positive, which indicates that complexation between HSA and phorate also involves hydrophobic interactions.

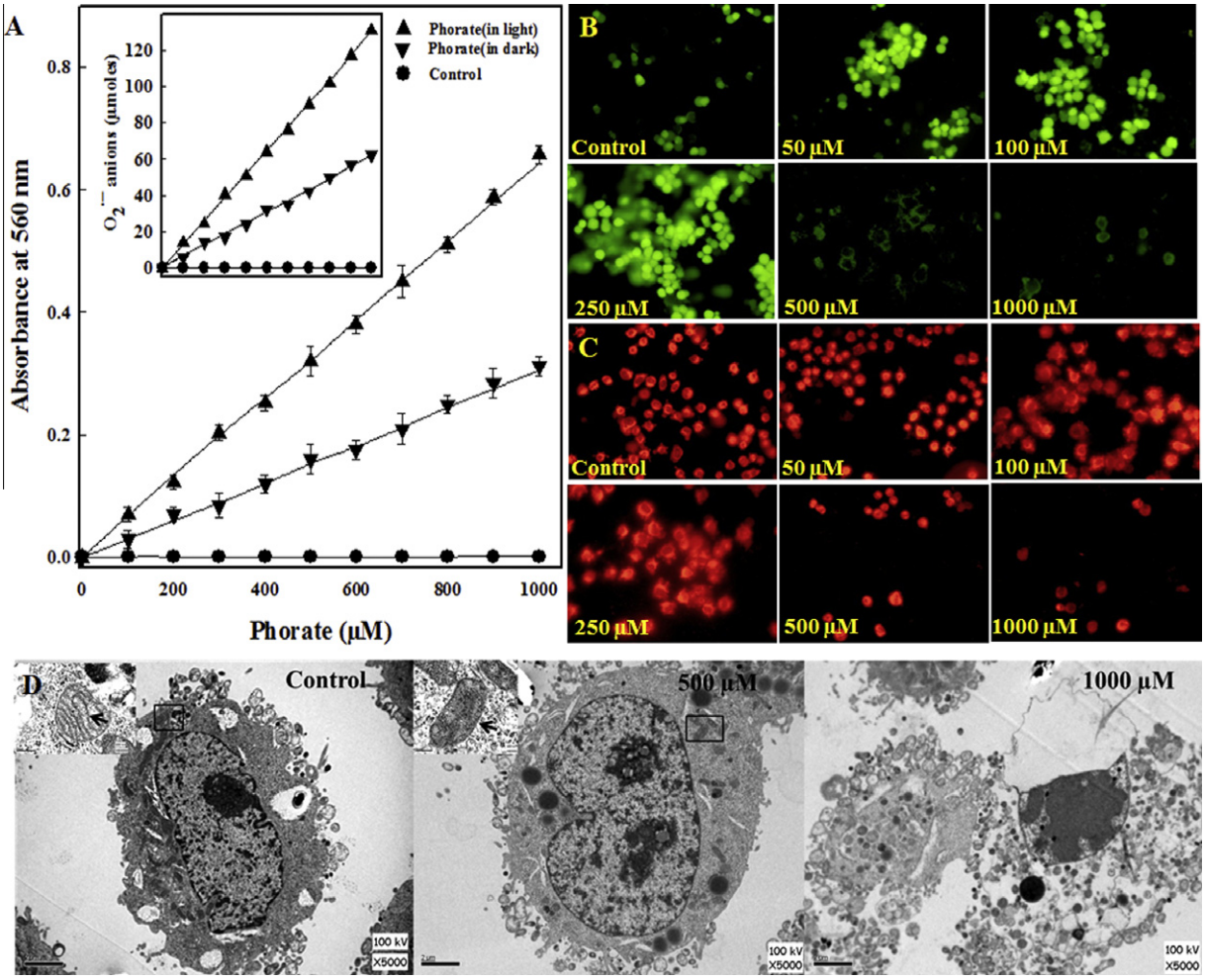

Fig. 10. Phorate induced ROS generation and mitochondrial damage. Panel A shows the extracellular superoxide anion ($O_2^{\cdot-}$) produced, plotted as the absorbance of a blue colored formazan product formed upon NBT reduction, as a function of phorate concentration. The inset depicts the absolute amounts of ($O_2^{\cdot-}$) anions generated in light and dark. Panel B shows the phorate concentration dependent enhancement in green fluorescence of DCF that occurs due to ROS generation up to 250 μM. Significant decrease in fluorescence at 500 and 1000 μM signifies the cell death due to necrosis. Panel C shows the reduction in the intensity of Rh123 fluorescent probe in phorate treated WISH cells. Panel D exhibit the representative TEM images indicating the cellular and mitochondrial changes in phorate treated WISH cells. Magnification 5000×; mitochondria in the inset at magnification 80,000× are indicated with arrows. (For interpretation of the references to color in this figure legend, the reader is referred to the web version of this article.)

The CD analysis of phorate–HSA complex demonstrated the changes in secondary structure of phorate treated HSA, even at much lower concentrations of 0.1 and 0.2 μM as compared to the amount used in fluorescence based studies. CD spectra of HSA exhibited characteristic features of the typical (α + β) helix structure of the free HSA and its phorate complex with negative peaks at 209 and 222–223 nm. The reasonable explanation is that the negative peaks between 208, 209 and 222–223 nm are contributed to $n \rightarrow \pi^*$ transfer for the peptide bond of α-helix. The binding of phorate to HSA caused a decrease in band intensity without any significant shift of the peaks, suggestive of conformational changes and a decrease in α-helical content of protein which corresponds with the reported changes in HSA native conformation upon binding with shikonin and a fungicide methyl thiophanate (He et al., 2005; Saquib et al., 2010a).

Phorate–HSA interaction also triggers the release of carbonyl and acid soluble amino groups, as protein hydrolysis products indicative of the protein damage. The protein degradation may occur due to peptide bond hydrolysis and/or chain scission at α-carbon position. The densitometric analysis of HSA on the polyacrylamide gel revealed a phorate concentration dependent decline in the band intensities. Indeed, no evidence was obtained for the presence of discrete fragments, however, the reaction of phorate with HSA results in the loss of parent protein via the formation of small random fragments. This corroborates with the results of Hawkins and Davies (1999), who have also reported the disappearance of HSA bands at much higher concentration of hypochlorite (HOCl) in SDS–PAGE analysis. The phorate induced protein damage and release of acid soluble residues could be attributed to excessive phorate binding and possible generation of reactive oxygen species (ROS) in vicinity of protein molecule. Davies et al. (1987) have reported gross structural modification and fragmentation in bovine serum albumin (BSA) upon exposure to ROS. Pesticide induced oxidative stress is reported to occur either through overproduction of free radicals or alteration in antioxidant defense mechanisms (Abdollahi et al., 2004). Therefore, in order to determine the phorate mediated oxidative damage, the *in vitro* production of both the extracellular and intracellular ROS have been assessed in phorate treated WISH cells. The results confirmed the ROS generating capability of phorate both extracellularly and intracellularly, possibly due to biochemical oxidation. Furthermore, the phorate induced oxidative stress in cells has been substantiated through TEM ultrastructural analysis of phorate treated cells. The loss of mitochondrial cristae in treated cells sug-

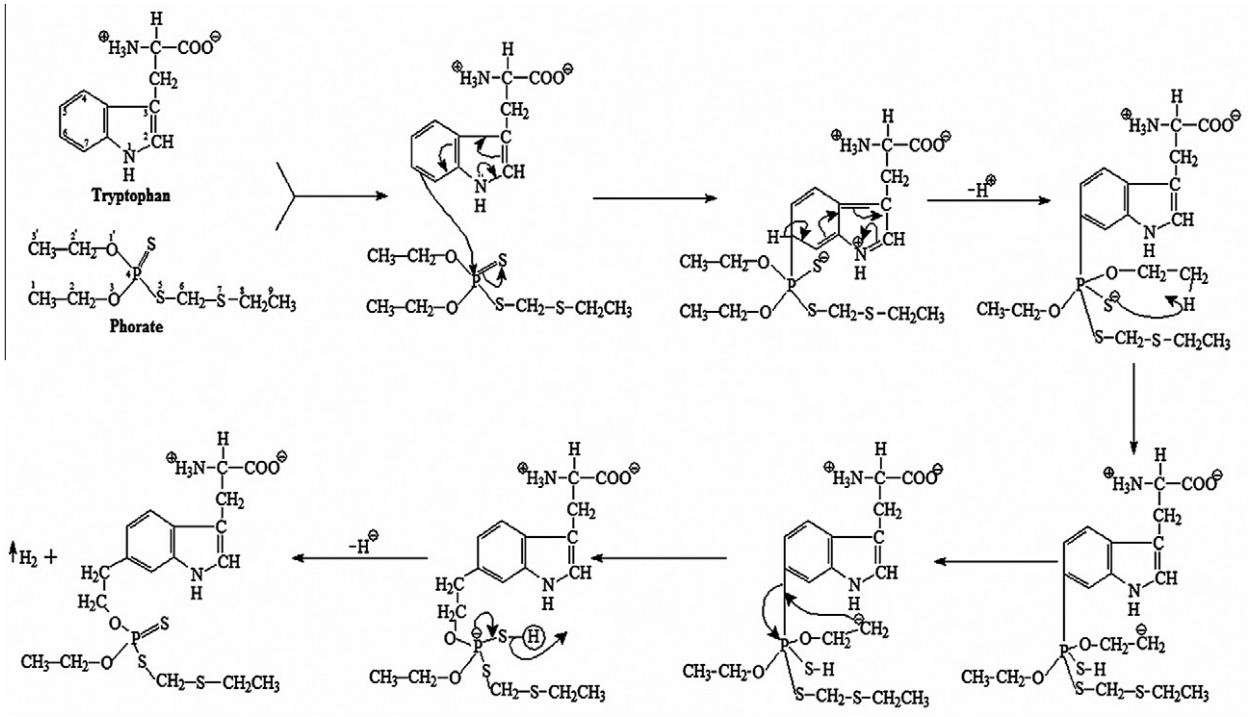

Scheme 1. Proposed mechanism of phorate–tryptophan interaction in HSA.

gests sub-cellular alterations typical of ROS induced mitochondrial damage, which clearly suggests phorate toxicity in exposed cells.

In conclusion, the fluorescence studies suggest a strong binding affinity of HSA for the insecticide phorate. The interaction predominantly occurs between the aromatic amino acids, preferably the Trp residue and the alkyl groups of phorate. The plausible mechanism suggests the involvement of resonating C-6 position on aromatic ring of tryptophan, as an electrophilic center. The electron deficient phosphorous moiety of phorate, due to attachment of two electronegative oxygen atoms, could be the preferred target. Most likely, the electrostatic substitution type reaction occurs following the intramolecular rearrangement that eventually link the 1′-O alkyl group of phorate at position 6 on aromatic ring of Trp 214 in sub-domain II A, as also explicitly demonstrated by docking analysis. The ability of phorate to generate ROS may also cause damage to cell membrane and mitochondria. Furthermore, the interaction of phorate with the physiologically important carrier protein (HSA) stipulates the possibility of developing insecticide-specific biosensors for biomonitoring and risk assessment from toxicological perspective.

Conflict of interest statement

The authors declare that there are no conflicts of interest.

Acknowledgment

Financial support through the Abdul Rahman Al-Jeraisy Chair for DNA Research, King Saud University, Riyadh, KSA, is greatly acknowledged.

Appendix A. Supplementary data

Supplementary data associated with this article can be found, in the online version, at doi:10.1016/j.fct.2011.04.028.

References

Abdollahi, M., Ranjbar, A., Shadnia, S., Nikfar, S., Rezaiee, A., 2004. Pesticides and oxidative stress: a review. Med. Sci. Monit. 10, 141–147.
Abert, W.C., Gregory, W.M., Allan, G.S., 1993. The binding interaction of Coomassie blue with proteins. Anal. Biochem. 213, 407–413.
Abhilash, P.C., Singh, N., 2009. Pesticide use and application: an Indian scenario. J. Hazard. Mater. 165, 1–12.
Alavanja, M.C.R., Samanic, C., Dosemeci, M., Lubin, J., Tarone, R., Lynch, C.F., Knott, C., Thomas, K., Hoppin, J.A., Barker, J., Coble, J., Sandler, D.P., Blair, A., 2003. Use of agricultural pesticides and prostate cancer risk in the agricultural health study cohort. Am. J. Epidemiol. 157, 800–814.
Berman, H.M., Westbrook, J., Feng, Z., Gilliland, G., Bhat, T.N., Weissig, H., Shindyalov, I.N., Bourne, P.E., 2000. The protein data bank. Nucleic Acids Res. 28, 235–242.
Chen, Y.H., Yang, J.T., Martinez, H.M., 1972. Determination of the secondary structures of proteins by circular dichroism and optical rotatory dispersion. Biochemistry 11, 4120–4131.
Chignell, C.F., 1972. Fluorescence spectroscopy-theory and measurement. In: Chignell, C.F. (Ed.), Methods in Pharmacology, vol. 2. Appleton-Century-Crofts, New York, pp. 1–32.
Davies, K.J.A., Delsignore, M.E., Lin, S.W., 1987. Protein damage and degradation by oxygen radicals. J. Biol. Chem. 262 (20), 9902–9907.
DeFerrari, M., Artuso, M., Bonassi, S., Bonatti, S., Cavalieri, Z., Pescatore, D., Marchini, E., Pisano, V., Abbondandolo, A., 1991. Cytogenetic biomonotiroing of an Italian population exposed to pesticides; chromosome aberration and sister-chromatid exchange analysis in peripheral blood lymphocytes. Mutat. Res. 260, 105–113.
Delano, W.L., 2004. The PyMOL Molecular Graphics System. DeLano Scientific, San Carlos CA, USA, <http://pymol.sourceforge.net/>.
Fulton, M.H., Key, P.B., 2001. Acetylcholinesterase inhibition in estuarine fish and invertebrates as an indicator of organophosphorus insecticide exposure and effects. Environ. Toxicol. Chem. 20, 37–45.
Hawkins, C.L., Davies, M.J., 1999. Hypochlorite-induced oxidation of proteins in plasma: formation of chloramines and nitrogen-centred radicals and their role in protein fragmentation. Biochem. J. 340, 539–548.
He, W., Li, Y., Tian, J., Liu, H., Hu, Z., Chen, X., 2005. Spectroscopic studies on binding of shikonin to human serum albumin. J. Photochem. Photobiol. A 174, 53–61.
Henderson, M.C., Kruger, S.K., Siddens, L.K., Stevenes, J.F., Williams, D.E., 2004. S-oxygenation of the thioether organophosphate insecticides phorate and disulfoton by human flavin-containing monooxygenase 2. Biochem. Pharmacol. 68, 959–967, <http://extoxnet.orst.edu/pips/phorate.htm> (Accessed on 22.05.10).
Hubbard, S.J., Thornton, J.M., 1993. 'NACCESS', Computer Program, Department of Biochemistry and Molecular Biology, University College, London.
Jaiswal, R., Khan, M.A., Musarrat, J., 2002. Photosensitized paraquat-induced structural alterations and free radical mediated fragmentation of serum albumin. J. Photochem. Photobiol. B 67, 163–170.

Kashyap, S.K., Jani, J.P., Saiyed, H.N., Gupta, S.K., 1984. Clinical effects and cholinesterase activity changes in workers exposed to phorate (Thimet). J. Environ. Sci. Health 19, 479–489.

Laemmli, U.K., 1970. Cleavage of structural proteins during the assembly of the head of Bacteriophage T4. Nature 227, 680–685.

Lappin, G.R., Clark, L.C., 1951. Colorimetric method for determination of traces of carbonyl compounds. Anal. Chem. 23, 541–542.

Li, J., Liu, X., Ren, C., Li, J., Sheng, F., Hu, Z., 2009. *In vitro* study on the interaction between thiophanate methyl and human serum albumin. J. Photochem. Photobiol. B 94, 158–163.

Mahajan, R., Bonner, M.R., Hoppin, J.A., Alavanja, M.C., 2006. Phorate exposure and incidence of cancer in the agricultural health study. Environ. Health Perspect. 114, 1205–1209.

Mahli, P.K., Grover, I.S., 1987. Genotoxic effects of some organophosphorus pesticides II. *In vivo* chromosomal aberration bioassay in bone marrow cells in rat. Mutat. Res. 188, 45–51.

Mansour, S.A., Belal, M.H., Abou-Arab, A.A.K., Gad, M.F., 2009a. Monitoring of pesticides and heavy metals in cucumber fruits produced from different farming systems. Chemosphere 75, 601–609.

Mansour, S.A., Belal, M.H., Abou-Arab, H.A.A.K., Ashour, M., Gad, M.F., 2009b. Evaluation of some pollutant levels in conventionally and organically farmed potato tubers and their risks to human health. Food Chem. Toxicol. 47, 615–624.

Moore, S., Stein, W.H., 1954. A modified ninhydrin reagent for photometric determination of amino acids and related compounds. J. Biol. Chem. 211, 907–913.

Morowati, M., 2001. Biochemical and histopathological changes in serum creatinine and kidney induced by inhalation of thimet (phorate) in male swiss albino mouse, Mus musculus. Env. Res. 87, 31–36.

Nakayama, T., Kinnura, T., Kodama, M., Nagata, C., 1983. Generation of hydrogen peroxide and superoxide anions from active metabolites of napthylamines and amino azo dyes: possible role in carcinogenesis. Carcinogenesis 4, 765–769.

Oruc, E.O., Usta, D., 2007. Evaluation of oxidative stress responses and neurotoxicity potential of diazinon in different tissues of Cyprinus carpio. Environ. Toxicol. Pharmacol. 23, 48–55.

Pagliuca, G., Serraino, A., Gazzotti, T., Zironi, E., Borsari, A., Rosmini, R., 2006. Organophosphorus pesticides residues in Italian raw milk. J. Dairy Res. 73, 1–5.

PMRAH, 2003. Pest Management Regulatory Agency Health, Proposed Acceptability for Continuing Registration, Canada. <http://dsp-psd.pwgsc.gc.ca/Collection/H113-18-2003-1E.pdf> (Accessed on 22.05.10).

Saquib, Q., Al-Khedhairy, A.A., Alarifi, S.A., Dwivedi, S., Mustafa, J., Musarrat, J., 2010a. Fungicide methyl thiophanate binding at sub-domain IIA of human serum albumin triggers conformational change and protein damage. Int. J. Biol. Macromol. 47, 60–67.

Saquib, Q., Al-Khedhairy, A.A., Singh, B.R., Arif, J.M., Musarrat, J., 2010b. Genotoxic fungicide methyl thiophanate as an oxidative stressor inducing 8-oxo-7, 8-dihydro-2′-deoxyguanosine adducts in DNA and mutagenesis. J. Environ. Sci. Health B 45, 1–6.

Siddiqui, M.A., Kashyap, M.P., Kumar, V., Al-Khedhairy, A.A., Musarrat, J., Pant, A.B., 2010. Protective potential of trans-resveratrol against 4-hydroxynonenal induced damage in PC12 cells. Toxicol. In vitro 24, 1592–1598.

Silva, D., Cortez, C.M., Bastos, J.C., 2004. Methyl parathion interaction with human and bovine serum albumin. Toxicol. Lett. 147, 53–61.

Sobti, R.C., Krishnan, A., Pffaffenberger, C.D., 1982. Cytokinetic and cytogenetic effects of some agricultural chemicals on human lymphoid cells *in vitro*: organophosphates. Mutat. Res. 102, 89–102.

Tang, J., Luan, F., Chen, X., 2006. Binding analysis of glycyrrhetinic acid to human serum albumin: fluorescence spectroscopy, FTIR, and molecular modeling. Bioorg. Med. Chem. 14, 3210–3217.

Tayyab, S., Khan, N.J., Khan, M.A., Kumar, Y., 2003. Behavior of various mammalian albumins towards bilirubin binding and photochemical properties of different bilirubin–albumin complexes. Int. J. Biol. Macromol. 31, 187–193.

Usmani, K.A., Karoly, E.D., Hodgson, E., Rose, R.L., 2004. In vitro sulfoxidation of thioether compounds by human cytochrome P450 and flavin containing monooxygenase isoforms with particular reference to the CYP2C subfamily. Drug Metab. Dispos. 32, 333–339.

Vandana, S., Zzaman, S., 1997. Phorate induced enzymological alterations in mouse olfactory bulb. Brain Res. Bull. 44, 247–252.

Wang, L., Liang, Y., Jiang, X., 2008. Analysis of eight organophosphorus pesticide residues in fresh vegetables retailed in agricultural product markets of Nanjing, China. Bull. Environ. Contam. Toxicol. 81, 377–382.

Yuan, T., Weljie, A.M., Vogel, H.J., 1998. Tryptophan fluorescence quenching by methionine and selenomethionine residues of calmodulin: orientation of peptide and protein binding. Biochemistry 37, 3187–3195.

Yuan, J.L., Iv, Z., Liu, Z.G., Hu, Z., Zou, G.L., 2007. Study on interaction between apigenin and human serum albumin by spectroscopy and molecular modeling. J. Photochem. Photobiol. A 191, 104–113.

Zambonin, C.G., Quinto, M., De Vietro, N., Palmisano, F., 2004. Solid-phase microextraction gas chromatography mass spectrometry: a fast and simple screening method for the assessment of organophosphorus pesticides residues in wine and fruit juices. Food Chem. 86, 269–274.

Zhang, G., Wang, Y., Zhang, H., Tang, S., Tao, W., 2007. Human serum albumin interaction with paraquat studied using spectroscopic methods. Pest. Biochem. Physiol. 87, 23–29.